Appl. Phys. B 82, 487–494 (2006)
DOI: 10.1007/s00340-005-2044-6

Applied Physics B
Lasers and Optics

C. JANSSEN✉
B. TUZSON

A diode laser spectrometer for symmetry selective detection of ozone isotopomers

Max-Planck-Institut für Kernphysik, Bereich Atmosphärenphysik, Saupfercheckweg 1, 69117 Heidelberg, Germany

Received: 6 July 2005/Revised version: 21 September 2005
Published online: 30 November 2005 •

ABSTRACT A tunable diode laser absorption spectrometer operating in the 10 μm range is described, which for the first time permits simultaneous detection and quantification of the five naturally most abundant ozone isotopomers: $^{16}O_3$, $^{16}O^{16}O^{18}O$, $^{16}O^{18}O^{16}O$, $^{16}O^{16}O^{17}O$, and $^{16}O^{17}O^{16}O$. Ozone samples of 25 μmole size are analysed with an estimated accuracy of 6‰ (2σ). This level of accuracy is demonstrated by comparing spectroscopically determined isotopologue enrichments of $^{16}O_2^{17}O$ and $^{16}O_2^{18}O$ with mass spectrometer measurements. Samples for the comparison were generated from natural oxygen in an electric discharge under two different pressure conditions. The precision obtained is sufficient to study both the isotopic and the symmetry dependence of the unique oxygen isotope anomaly in ozone formation, which shows isotopomer specific fractionation values well in the 10% range.

PACS 42.60.By; 42.55.Px; 33.20.Ea

1 Introduction

Ozone (O_3) gains its special importance from the role it plays in atmospheric chemistry. Its spectral properties make it a unique absorber in the UV, that protects the Earth's surface from harmful solar irradiation. In addition, the ozone molecule is pivotal in atmospheric oxidation. Not only is it an efficient oxidizer, it is especially important as a precursor molecule for primary atmospheric oxidants, such as the hydroxyl (OH) or the nitrate radical (NO_3).

Besides being a prominent molecule in the chemistry of the atmosphere, the physics of its formation appears to be exceptional too: a possibly unique and unusually large isotope effect was found in the ozone formation reaction [1]

$$O + O_2 + M \rightarrow O_3 + M\,. \qquad (1)$$

This reaction shows a surprisingly large variation of up to 60% in the rate coefficients, when different isotopic variants are considered [2, 3]. Originally, the effect was discovered in the atmosphere [4] and later confirmed in numerous laboratory measurements. It still is the subject of many experimental and theoretical efforts (see for recent reviews [5–7]). In both the atmosphere and the laboratory, large (∼ 10%) and almost equal enrichments of the heavy oxygen isotopes ^{17}O and ^{18}O in ozone are observed [1, 8, 9]. The magnitude of the enrichment exceeds that of other atmospheric gases and oxygen bearing compounds on Earth [6, 10], making ozone the most heavily enriched natural oxygen containing substance.

One persistent question is, how the oxygen isotope enrichment is shared between the asymmetric and symmetric isotopomers of ozone? Since the ozone molecule has an isosceles triangular geometry, substitution with the rare stable isotopes either leads to symmetric (e.g. $^{16}O^{17}O^{16}O$ and $^{16}O^{18}O^{16}O$) or asymmetric (e.g. $^{16}O^{16}O^{17}O$ and $^{16}O^{16}O^{18}O$) molecules, which belong to the C_{2v} or C_s point groups, respectively. Not only is the intramolecular distribution of heavy oxygen in $^{16}O_2^{17}O$ or $^{16}O_2^{18}O$ an important detail of the ozone isotope effect, but knowledge of this distribution is also required to understand the molecular-level details of isotope transfer from ozone into other atmospheric species [11], that has been observed in N_2O (e.g. [12]) and stratospheric CO_2 (e.g. [13]). Understanding these details is essential for identifying the chemical pathways that lead to the observed isotope anomalies in these two molecules.

So far, only a few precise symmetry selective measurements have been performed. Most of these were concerned with the more abundant isotopomers of mass 50 u and only one [14] out of six atmospheric studies reports 2σ errors clearly smaller than 10%, which appears to be the minimum requirement to study atmospheric effects. Recently it was shown that laboratory studies in the mid-IR, based on tunable diode laser absorption spectrometry (TDLAS) [15, 16] as well as Fourier transform spectroscopic investigations of $^{16}O^{16}O^{18}O$ and $^{16}O^{18}O^{16}O$ in the far-IR [17] agree, when temperature effects are taken into account [11]. Experimental evidence on $^{16}O^{16}O^{17}O$ and $^{16}O^{17}O^{16}O$ however, is still uncertain, because the only symmetry selective study available [18] suffers from errors (2σ) in the range of the measurement values.

Symmetry specific measurements of isotopomer abundances are the natural resort of infrared absorption spectroscopy, because – unlike the more common and precise mass spectrometry (MS) – the technique can inherently differentiate between structural isomers of the same isotopologue. In the effort to tackle the aforementioned open questions we

✉ Fax: +49-6221-516-324, E-mail: c.janssen@mpi-hd.mpg.de

have developed a TDLAS that allows simultaneous measurement of the naturally occurring ozone isotopomers in the mid-IR. Compared to isotope selective absorption spectroscopy of stable greenhouse gases (e.g. CH_4, N_2O, CO_2 and H_2O), where a precision on the sub per-mil level has been well reached [19–23], the reactivity of the ozone molecule and the lack of a common isotope standard substance pose challenges that require special precaution and make it difficult to achieve a similar level of precision. Due to the sizable isotope effect in ozone formation, however, an accuracy in the few per-mil range is entirely sufficient.

In this paper, we describe a TDL based spectrometer for symmetry selective investigation of monosubstituted ozone isotopomers. The experimental setup as well as the details of line selection and spectrum analysis are provided in the next section, with a special emphasis on requirements due to the reactivity of the ozone molecule. We then present measurements on ozone samples that were produced in an electric discharge in oxygen. Finally, by deriving total isotopologue enrichments from the isotopomer measurements, the performance of the absorption spectrometer is demonstrated in a comparison with the results from a mass spectrometer.

2 Experimental

2.1 *Spectrometer setup and characterisation*

Depending on the spectral region of interest, several laser based light sources are available in the mid-IR, which have successfully been employed for isotope selective absorption spectroscopy: difference frequency generation, lead-salt and antimonide diodes, direct solid state lasers, gas lasers and quantum cascade lasers (QCL) [24]. The latter are particularly attractive, because of their narrow line width and near room temperature operating conditions. Among the tunable solid state lasers, the narrow tuning range of the QCL ($\sim 3\,\mathrm{cm}^{-1}$), however, renders them less versatile than lead salt diodes, that emit over a broader range ($\sim 100\,\mathrm{cm}^{-1}$) [25]. These extended survey capabilities were the determining factor for a decision in favor of a tunable diode laser based spectrometer – even more so, because liquid nitrogen cooling is not a real constraint in a laboratory environment.

The general setup of the laser spectrometer has already been described elsewhere [26]. Here we give a brief overview and focus on details that are essential for the accurate determination of ozone isotopomer abundance ratios.

The custom made optical system (Aerolaser/Laser Photonics) including laser diodes, dewars, detectors, preamplifiers and the electronic control unit was modified to improve the signal-to-noise ratio and is presented in Fig. 1.

A 0.3 mW lead-salt diode (model 5621-1000, Laser Photonics), operating in single mode emission, is used as the source for laser radiation in the range from 1000 to $1060\,\mathrm{cm}^{-1}$. Frequency tuning rates of about $\mathrm{d}\nu/\mathrm{d}T = 3.8\,\mathrm{cm}^{-1}/\mathrm{K}$ and $\mathrm{d}\nu/\mathrm{d}I = 3.4\times10^{-2}\,\mathrm{cm}^{-1}/\mathrm{mA}$ have been determined for the particular diode used. The operating temperature around 80 K is maintained by electronic heating of the diode inside a large LN_2 dewar. The emitted radiation is collimated by an off-axis parabolic mirror and a modified mechanical chopper (model SR540, Stanford Research Systems) modulates the beam intensity with a frequency of roughly 1 kHz. A wedged BaF_2 crystal is used as a beam splitter. The transmitted beam is coupled into an astigmatic mirror multi-pass absorption cell (model 5612, New Focus) at $f/\# = 60$. A 90-pass configuration with about 50 m path length was chosen in the 3.21 cell that has a base length of roughly 55 cm. The standard cell mirrors were replaced by two mirrors with surface quality parameters (scratch dig) 20–10 (Aerodyne Research). Both mirrors have been rotated by 120° with respect to the standard New Focus mounting configuration in order to maximize the distance between closest laser spots and the coupling hole on the front mirror [27]. These modifications reduced the optical fringes level from $\sim 5\times10^{-3}$ down to $< 4\times10^{-4}$ over the entire mode width of $1\,\mathrm{cm}^{-1}$. The Ni-metal coatings on Al-plates and mirror holders inside the pyrex cell were passivated by a 5 μm gold layer. This led to an extended 1/e-residence time of ozone of about 33 hours at a typical ozone sample pressures of 16 Pa. The cell output beam is focused onto a detector diode. The photo-current is first pre-amplified, then detected using phase sensitive detection (model SR830, Stanford Research Systems) and finally recorded by a multi purpose data acquisition card (PCI-MIO-16XE-50, National Instruments) onboard a PC.

The secondary beam passes through a spherical confocal Fabry–Pérot etalon (model AL6000, AeroLaser) with a free spectral range FSR $= (8.025 \pm 0.001)\,10^{-3}\,\mathrm{cm}^{-1}$. Together with absolute line positions [28, taken from the HI-

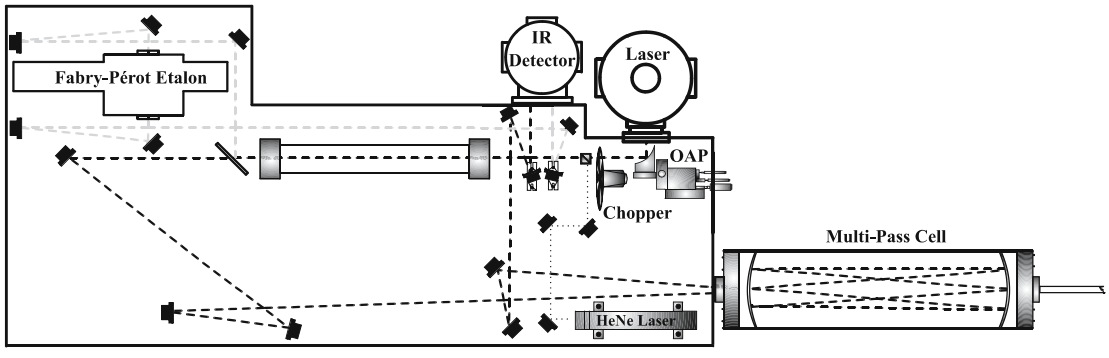

FIGURE 1 Scheme of the optical setup. Following the main laser beam (*dark dashed line*), the components are laser dewar, off-axis parabolic (OAP) mirror, mechanical chopper, moveable reference gas cell, beam splitter, collimating optics, an astigmatic mirror multi-pass cell, collimating optics and IR detector dewars. The reference beam (*grey dashed line*) passes through a confocal Fabry–Pérot etalon. Also indicated is a HeNe laser for the alignment of the optical components (*dotted line*)

TRAN 2004 database] of typically five to seven strong $^{16}O_3$ lines within the 1 cm^{-1} diode laser scanning range an accurate frequency scale is provided. The inherent consistency of this approach as well as a comparison with an independent frequency scale that is based on lines of different CO_2 isotopologues resulted in an overall frequency accuracy of $\Delta\nu = 5 \times 10^{-5}$ cm^{-1} [26].

2.2 *Sample preparation and measurement*

Ozone was produced by electric discharge in natural oxygen (research grade with 99.9995% purity, Messer Griesheim). Oxygen gas was flown either near 140 hPa or at 1 hPa through an U-shaped glass tube with inner diameter and length of 10 mm and 75 cm, respectively. Two copper ring electrodes are attached to the outside of the tube and connected to a radio frequency high voltage generator (custom made, ATPE). Downstream of the U-tube a cold trap is installed, that can be kept at temperatures between 64 and 78 K. Due to its low vapor pressure, ozone produced in the discharge condenses inside the cold finger, while molecular oxygen remains in the gas phase and is pumped away. After collection, trapped ozone can be released into the multipass cell for spectroscopic analysis. Following the analysis, the gas is transferred to a small stainless steel tube (8 mm inner diameter, 15 cm length) which is immersed in liquid helium. After that the tube is brought to room temperature and surface decomposition reactions then lead to a complete conversion of the ozone sample into molecular oxygen. This way the overall isotopic composition of ozone can be determined with a small (1.5 inch) Mattauch–Herzog type mass spectrometer (e.g. [29]), originally designed for operation in space research. In order to check the accuracy of this instrument, ozone samples with varying isotopic compositions were prepared under similar conditions and, after conversion to molecular oxygen, analysed by the small MS as well as by a high precision isotope ratio MS (Delta^{XL}Plus, ThermoQuest Finnigan).

Three portions of ozone sample and reference gases were prepared under almost the same high and low pressure conditions, respectively. For the samples, the pressure in the oxygen discharge was fixed at 140–147 hPa and sampling was performed within 2 minutes. Ozone gas used as a reference was prepared with the same setup at oxygen pressures between 0.98 and 1.05 hPa. In order to collect the same amount of ozone under the low pressure conditions a collection time of 2.5 hours was required. Immediately after ozone production and cryogenic separation from oxygen, the ozone gas was admitted to the multi-pass cell and the laser measurements were started. The ozone pressure in the multi-pass cell was between 15 and 17 Pa for both the sample and the reference gas analysis. This corresponds to a sample size of somewhat less than 25 μmole.

Spectra, that contained 3000 data points, were repeatedly recorded in a selected spectral window of about 1 cm^{-1} width. Recording of a single spectrum took about 45 s. Fifteen minutes were thus required to acquire a sequence of twenty spectra. After that the laser temperature had to be changed for emission in a different mode and only after 10 more minutes that were required to achieve stable temperature conditions, a new sequence of spectra were taken in another spectral window. A typical sample analysis in three different spectral regions thus took one hour. This is still significantly shorter than the ozone decay time of 33 hours in the absorption cell.

2.3 *Line selection and analysis*

Due to the ν_3 band of ozone at 10 μm being the strongest fundamental, it is best suited for sensitive and symmetry resolved detection of ozone isotopomers. In that region, the ozone spectrum is quite dense. This implies that there are always many lines within the tuning range of the laser diode, however, this requires a careful selection of lines that are free from interference with other transitions. The measurement of the rare isotopomers with ^{17}O and ^{18}O is particularly challenging in a one-path optical arrangement, such as the one described here. The relative abundances of the ozone species in the atmosphere ($^{16}O_3$, $^{16}O^{16}O^{18}O$, $^{16}O^{18}O^{16}O$, $^{16}O^{16}O^{17}O$ and $^{16}O^{17}O^{16}O$ occur roughly in proportions of 2630 : 10 : 5 : 2 : 1) strongly favor the absorption lines of $^{16}O_3$ (see also Fig. 2).

In order to guarantee unambiguous and quantitative determination of isotopic ratios, all of the following conditions should be fulfilled simultaneously: strong lines of all the rare isotopomers have to be available within the accessible range of the laser diode and the lines of the more abundant species must have similar absorbances. Ideally, they should be located within a single laser mode and there must be no interference from other transitions of the same or of other species.

Figure 2 shows the spectral regions that are particularly attractive under these conditions. The different branches of the dominant type A band transitions can be well recognised. The Q-branches of $^{16}O_3$ appear to have a high energy cut-off at around 1042.3 cm^{-1}, beyond which Q-branch transitions become very sparse. Over and above, R-branch transitions of $^{16}O_3$ are weak in the region up to 1044 cm^{-1}, because of the

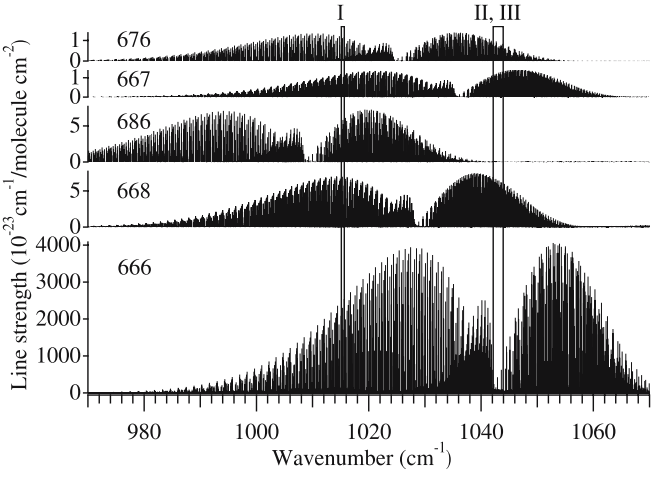

FIGURE 2 Spectra of the most abundant natural ozone isotopomers in the ν_3 ro-vibrational band region. Line strengths were multiplied by the natural abundance of the isotopomers to scale with absorption signals. The weighting by abundance is already included in the definition of line strengths used by the HITRAN 2004 database [28], from where the data were taken. Spectral windows where the measurements were performed are indicated by rectangles. I: 1015.1–1015.9 cm^{-1} and the overlapping regions II and III: 1042–1044 cm^{-1}

marginal thermal population of the lower states. At the same time, all the heavy isotopomers except $^{16}O^{18}O^{16}O$ have significant absorption there. For the measurement of $^{16}O^{16}O^{18}O$, $^{16}O^{16}O^{17}O$ and $^{16}O^{17}O^{16}O$, interference from the main absorbing species is thus minimized in the 1042–1044 cm^{-1} region, which could be assessed in the spectral windows II and III by our laser diode. One more region (I) in the *P*-branches of $^{16}O_3$ was selected. Clearly, the *P*-branch region of $^{16}O_3$ is more appealing than the *R*-branches, because the isotope shift moves the heavy isotopomers into that direction and the spacing between rotational levels is less dense there than in the *R*-branches. In window I around 1015 cm^{-1} all heavy isotopomers can be detected and in particular $^{16}O^{18}O^{16}O$ is most efficiently measured due to the window being close to the absorption maximum in the *R*-branches of this species.

The three spectral regions I–III that were identified by a survey of the HITRAN 2004 database were carefully investigated with the TDL before they were finally used for isotopic analysis. This assured us that the ozone isotopomers are uniquely identified by their transitions and that there is negligible overlap between different lines. As a consequence, line positions of favourable ozone isotopomer transitions reported in the current version of the HITRAN database could be checked. Generally – and only with very few exceptions – the database record agreed well with our observations. For example, from a total of 30 $^{16}O_3$ lines with intensities in the 3×10^{-24}–2×10^{-22} cm^{-1} cm^2/molecule range (not necessarily restricted to the spectral range used for the isotopic evaluation), only two lines were off by 6 and 16×10^{-4} cm^{-1}, respectively. The shifts of the remaining 28 lines with respect to the database almost follow a normal distribution with a mean of 0.4×10^{-4} cm^{-1} and a standard deviation of 1.4×10^{-4} cm^{-1}. This is a remarkable agreement given that line positions in the database are generally specified with a precision of 4 digits only. Some $^{16}O^{17}O^{16}O$ transitions, however, were found to be shifted systematically by as much as 4×10^{-3} cm^{-1} [26].

Details about the selected lines are provided in Table 1. With 17 lines, most information is available on $^{16}O^{16}O^{18}O$, followed by $^{16}O^{16}O^{17}O$ and $^{16}O^{17}O^{16}O$, where 10 and 8 lines have been used, respectively. Least information is on $^{16}O^{18}O^{16}O$, where only 5 lines were employed. In principle, the situation may be improved at the price of an extended measurement time when one allows for analysis in additional spectral windows. For demonstrating the ability of simultaneous measurement of all naturally occurring ozone isotopomers, however, the number of five lines is already sufficient. Also, because the asymmetric species are expected to be important for isotope transfer chemistry, it must be considered advantageous that more lines are available for the detection of those molecules.

Quantitative analysis of the spectra was carried out with the Igor Pro software (wavemetrics), which includes a multipeak fitting package based on the Levenberg–Marquardt minimisation algorithm. Using a Gaussian line profile, between one and eight lines were simultaneously fitted in one of several microwindows together with a third order polynomial baseline. An illustration of the fitting procedure is given in Fig. 3. Eight lines were simultaneously fitted in the range between 1042.687 and 1042.734 cm^{-1}. Since accurate know-

SW	TYPE	ν_{obs}	ν_{HIT04}	$\Delta\nu$	E''	S
I	666	1015.20803	1015.2080	0	1458.4679	2.712
	666	1015.22400	1015.2241	1	1199.4461	11.350
	666	1015.30029	1015.3003	0	1077.7052	4.433
	666	1015.46810	1015.4680	−1	1236.8368	9.808
	666	1015.53179	1015.5317	−1	330.4966	0.935
	666	1015.54576	1015.5458	0	1606.8394	1.471
	666	1015.55849	1015.5585	0	1062.7116	8.067
	666	1015.70087	1015.7008	−1	1046.0256	7.298
	667	1015.80095	1015.8009	−1	195.5553	1.163
	676	1015.74998	1015.7496	−4	85.6116	0.690
*	668	1015.27101	1015.2712	2	301.4883	1.254
	686	1015.17198	1015.1720	0	55.9812	4.596
	686	1015.22738	1015.2274	0	109.3569	3.327
	686	1015.41641	1015.4163	−1	29.9618	5.846
	686	1015.45999	1015.4599	−1	41.7431	5.269
	686	1015.75548	1015.7554	−1	33.9264	5.712
II	666	1042.36051	1042.36113	6	1516.8623	3.076
	666	1042.55065	1042.5507	1	1816.5079	1.452
	666	1042.55652	1042.55657	1	112.5424	0.456
	666	1042.63211	1042.6320	−1	1969.0298	2.404
	666	1042.70816	1042.7081	−1	2213.8716	0.729
	666	1042.71636	1042.7162	−2	1887.7153	3.298
	666	1042.72748	1042.7273	−2	2089.8353	1.317
	667	1042.49779	1042.4980	2	38.6983	1.183
	667	1042.50771	1042.5077	0	64.7188	0.971
	667	1042.51274	1042.5127	0	64.7225	0.971
	667	1042.70241	1042.7026	2	49.1265	1.096
	676	1042.66810	1042.6703	22	326.1093	0.783
	676	1042.69217	1042.6944	22	268.4824	0.957
	676	1042.73013	1042.7322	21	301.6402	0.861
*	668	1042.20545	1042.2051	−4	549.2602	2.442
	668	1042.23073	1042.2308	1	196.5825	6.385
	668	1042.26472	1042.2648	1	165.2646	6.615
	668	1042.34455	1042.3435	−11	278.2073	1.500
	668	1042.54650	1042.5466	1	214.5516	6.115
III	666	1042.99335	1042.99348	1	1357.4944	5.816
	666	1043.05701	1043.0567	−3	1914.4399	2.923
	666	1043.15693	1043.1573	4	1812.3974	4.769
	666	1043.26643	1043.2664	0	1597.2988	1.058
	666	1043.35887	1043.3589	0	1427.0171	11.920
	666	1043.36271	1043.3626	−1	1923.1818	2.856
	666	1043.70280	1043.7029	1	2018.2303	1.740
	667	1043.16072	1043.1610	3	40.8594	1.183
	667	1043.20618	1043.2061	−1	72.8872	1.038
*	667	1043.25609	1043.2561	0	283.9485	0.775
*	667	1043.28694	1043.2868	−1	175.3830	1.263
	667	1043.76479	1043.7650	2	55.2750	1.317
	676	1043.18901	1043.1915	25	415.7044	0.516
	676	1043.20283	1043.2053	25	344.3724	0.722
	676	1043.67185	1043.6750	32	497.8245	0.366
	676	1043.76848	1043.7723	38	661.3738	0.174
	668	1042.95484	1042.9546	−2	296.4963	4.000
	668	1042.99878	1043.0001	13	296.4977	2.423
*	668	1043.01157	1043.0118	2	699.1268	0.459
	668	1043.07050	1043.0707	2	232.5346	5.808
*	668	1043.25150	1043.2516	1	871.2814	0.563
*	668	1043.35405	1043.3539	−2	429.7911	4.520
	668	1043.41292	1043.4128	−1	268.8857	4.654
	668	1043.44042	1043.4404	0	230.3679	5.731
	668	1043.53141	1043.5314	0	198.5708	6.192
	668	1043.67957	1043.6796	0	208.0322	6.154
	668	1043.79114	1043.7914	3	271.6699	5.154

TABLE 1 The 62 ozone absorption lines used for the isotopic investigation. Isotopomers are indicated by their respective AFGL codes ($6 = ^{16}O$, $7 = ^{17}O$, and $8 = ^{18}O$), introduced by the Air Force Geophysical Laboratory. Measured and tabulated line positions ν_{obs} and ν_{HIT04} (in cm^{-1}) in the three spectral windows (SW), as well as the observed differences, $\Delta\nu = \nu_{HIT04} - \nu_{obs}$, (in $10^{-4}cm^{-1}$) are given. Lower state energies E'' (in cm^{-1}) and line strengths S (in $10^{-23}cm^{-1}cm^2$/molecule) are from the HITRAN 2004 database [28]. Degenerate transitions, where individual line strengths have been added, are indicated (*)

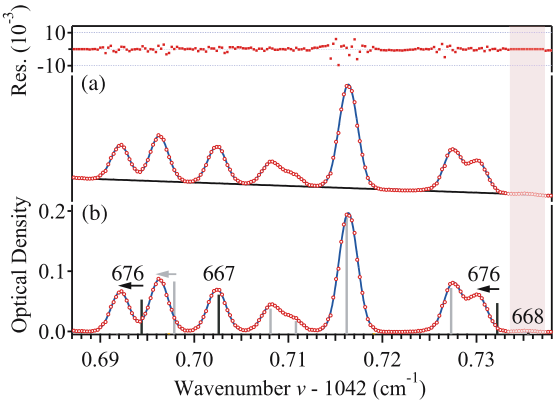

FIGURE 3 Section of spectral window II. The direct and the baseline corrected spectrum (*open circles*) and a fit (*solid line*) are shown in panels (**a**) and (**b**), respectively. Panel (**a**) shows the simultaneously fitted polynomial baseline, that is subtracted in panel (**b**) for comparison purposes. The quality of the fit can be assessed from the residuals in the top panel. Enhanced residual signals at the edges of lines are due to short-time frequency instabilities caused by temperature fluctuations in the laser diode. Line positions according to the HITRAN 2004 database are indicated by *vertical sticks*: $^{16}O_3$ – *grey*, heavy ozone – *black* and additionally labelled by the AFGL codes 667, 676 and 668, respectively. *Horizontal arrows* indicate a shift with respect to the database. The *shaded region* is excluded from the analysis

ledge of the baseline is crucial, it is defined by including absorption free portions of the spectrum outside the microwindow within a $\sim 0.4\,\mathrm{cm}^{-1}$ range. As mentioned before, line positions of $^{16}O^{17}O^{16}O$ show a significant shift with respect to HITRAN 2004, whereas other species generally agree well. The mismatch between the observed transition of $^{16}O_3$ at $1042.6963\,\mathrm{cm}^{-1}$ and the corresponding database entry at $1042.69787\,\mathrm{cm}^{-1}$ (Fig. 3) appears to be a rare exception.

Measurements of isotopomer ratios by absorption spectroscopy rely on the Beer–Lambert law

$$\tau = -\ln\left(I/I_0\right) = \sigma n l\,, \tag{2}$$

which relates the attenuation of light (I and I_0 being the transmitted and incident intensity, respectively) to the particle density n of a uniformly distributed absorber along the light path of length l. In this equation the optical density τ is introduced and σ denotes the cross section of the absorber which, apart from line broadening effects, is a molecular characteristic and can be considered as a constant in this experiment. More explicitly, when a heavy isotopomer $X = (^{16}O^{16}O^{18}O,\ ^{16}O^{18}O^{16}O,\ ^{16}O^{16}O^{17}O,\ ^{16}O^{17}O^{16}O)$ is enriched in a sample (S) with respect to a reference (R) gas

$$\varepsilon(X) = \frac{\left([X]/[^{16}O_3]\right)_\mathrm{S}}{\left([X]/[^{16}O_3]\right)_\mathrm{R}} - 1\,. \tag{3}$$

The enrichment ε may be expressed in terms of the optical densities τ of the heavy isotopomers (X) and of the main species ($^{16}O_3$) as

$$\varepsilon(X) = \frac{\left\{\tau\left(X\right)/\tau\left(^{16}O_3\right)\right\}_\mathrm{S}}{\left\{\tau\left(X\right)/\tau\left(^{16}O_3\right)\right\}_\mathrm{R}} - 1\,, \tag{4}$$

when the substitution $n = \tau/(\sigma l)$ is performed. In (4) the length of the light path has cancelled, because it is identical for all isotopomers in each of the measurements. Furthermore, cancellation of the isotopic cross sections occurs, when temperature and pressure conditions are the same for sample and reference measurements. This is due to line strength and line shape function for each of the isotopomers being the same in the two measurements. Slight differences in pressure and temperature can be and are nevertheless, accounted for as corrections to the above formula. Pressure variations, however, are of minor importance here, because the measurements are performed in the Doppler limit, where the pressure is proportional to the absorption signal. Due to small absorptions (typically $\tau = 5\%$–10%, and between 5 and 70% for $^{16}O_3$ only), saturation effects are small. This is demonstrated twofold. First, absorption measurements with varying ozone concentrations didn't show any significant departure from linearity and, second, the comparison with MS measurements presented later in Sect. 3.2 confirms that conclusion.

Note here, that our definition of an enrichment (in (3)) deviates from the one usually employed. Commonly the isotopic composition of ozone is referenced to a calculated standard that derives from the isotopic composition of molecular oxygen out of which the ozone is formed (e.g. [7]). In the case of atmospheric samples the reference gas composition would be determined from oxygen in air. The calculated composition of the standard, which frequently is referred to as "statistical" or "calculated" ozone, reflects the isotope composition of the molecular oxygen and includes factors to account for combinatorial differences in the statistical distribution of isotopes within a tri-atomic (O_3) and a diatomic (O_2) molecule. Due to large ($\sim 10\%$) systematic uncertainties in the line strengths of individual ozone isotopomers [11, 30], however, a comparison with a calculated standard would introduce these line strength uncertainties that are unacceptably large. Therefore, ozone samples are compared with ozone, where the essential features of the ozone isotope effect have been "switched off". Ozone that is formed under low pressure conditions in an electric discharge [16, 31] has this particular property and it was therefore used as a reference gas here. This way systematic uncertainties in the line strengths did not enter into the determination of the isotopomer specific fractionation values.

Equation (4) holds for each suitable pair of absorption lines. In principle, all measured lines should be used to determine ε. The finite life time of ozone in the multi-pass cell in combination with the successive measurement in different spectral regions, however, requires some care in the evaluation of $\varepsilon(X)$. Only pairs of lines recorded in the same spectral window (and thus within 45 s) are suitable for quantitative analysis, because within one hour typically 3% of the original ozone sample will be decomposed such that the comparison of absorption signals measured at the beginning and at the end of a recording cycle suffers from this degradation. Because $^{16}O^{18}O^{16}O$ lines are only measured in the first spectral window at the beginning of the recording sequence, a comparison with absorptions of $^{16}O_3$ measured in the last spectral window (III) would imply that a bias of almost 3% is introduced in the derived $[^{16}O^{18}O^{16}O]/[^{16}O_3]$-ratio. Despite some degree of cancellation of this degradation effect, there is no complete elimination upon dividing individual absorption signals from sample and reference even when the reference ozone is measured following the measurement protocol for the sam-

Sample	$\varepsilon(668)$	$\varepsilon(686)$	$\varepsilon(667)$	$\varepsilon(676)$
1	25.0(3)	5.2(3)	20.0(4)	2.7(2)
2	24.4(2)	5.9(5)	19.6(3)	3.2(3)
3	24.8(2)	4.8(2)	20.1(3)	2.6(2)
$\overline{\varepsilon(X)}$	24.7(3)	5.3(5)	19.9(3)	2.8(3)

TABLE 2 Isotopomer specific enrichments ε (in %) of three ozone sample/reference pairs generated in electric discharges. Standard deviations of individual measurements are estimated from the scatter in the data and are given in parentheses. Average values are shown in the last line and standard deviations given there refer to the scatter of the three independent measurements. Isotopomers are designated by their respective AFGL codes

ple. One reason is that the dead times required for temperature adjustment of the laser diode are manually selected and therefore are different. Time shifts of only ten minutes between the two recording sequences of sample and reference ozone alone lead to artificial fractionation effects in the 5‰ range when lines from different windows are used for the evaluation. Furthermore, the ozone decomposition rates depend on the actual surface condition, and vary in the measurements of sample and reference. This also prevents a complete cancellation.

The data evaluation procedure was thus to calculate ratios τ_S/τ_R at the center of each line within a selected window first, and then to average over all ratios available for X and $^{16}O_3$, separately. From these two averages, the ratio of optical densities in (4) is obtained – again for each window individually. The measurement result $\varepsilon(X)$ is finally obtained by averaging over all spectral windows. The validity of this approach was checked by repeated measurements in the first window after a complete cycle. Within the errors, the results from the repeated measurements were identical with the first. This is in agreement with the observed ozone decay times of 33 hours and expected isotope effects for volume based wall decomposition, that are controlled by thermal velocities. The time scale for kinetic fractionation of residual $^{16}O^{16}O^{18}O$ and $^{16}O^{18}O^{16}O$ is thus of the order of 67 days ($\approx 33\,\text{hours}/[(50/48)^{0.5}-1]$). This renders isotope effects due to heterogeneous ozone decomposition in the cell negligible (< 1‰) within the one hour measurement period.

3 Spectrometer performance

3.1 *Ozone isotopomer enrichments*

Table 2 shows the results of the spectroscopic analysis for the three sample and reference pairs. Large 20%–25% effects are observed in the asymmetric molecules. On the contrary, the symmetric species are only slightly enriched ($< 6\%$); the heavier one, $^{16}O^{18}O^{16}O$, about twice as much as the lighter $^{16}O^{17}O^{16}O$ molecule. The results for $^{16}O^{16}O^{18}O$ are in reasonable agreement with a previous TDLAS study restricted to ^{18}O containing ozone [16], where about 21% enrichment was found. Temperatures there were likely lower due to electrodes reaching inside the reactor. This causes less ohmic heating than the use of outside lying electrodes. However, a slight, but substantial enrichment of the symmetric molecule by about 9% was also reported. The origin of the higher enrichment found for $^{16}O^{18}O^{16}O$ in the earlier experiment remains yet unexplained, because no strong temperature dependence is expected in the formation of symmetric molecules [11]. Either the isotopic chemistry of ozone in a discharge is more complex than thought previously [1, 16, 32], which would question the direct applicability of discharge based experiments to explain the ozone isotope anomaly, or its T-dependence is more complex than expected. Clearly, more investigations are required, and experiments that avoid the use of an electric discharge to generate oxygen atoms would be particularly attractive. The large difference between the isotopic enrichments of symmetric and asymmetric species, however, provides an experimental means to unambiguously assign absorption features to a certain species [26].

For each isotopomer, the precision of the measurement could be estimated from the scatter in the ratio of optical densities between sample and reference τ_S/τ_R, that propagates into the calculated enrichment value. The reported uncertainties reflect this scatter and are calculated as the internal errors of a weighted average over all spectral windows. This number agrees with the observed statistical fluctuations of the individual optical densities in the 20 repeated scans. Furthermore, the error estimate compares favorably with the standard deviation (σ_{n-1}) of the three measurements given in the last line of Table 2. A typical uncertainty of 0.3% may be derived from this. Only for $^{16}O^{18}O^{16}O$, for which the least number of lines exist, the error might be slightly larger. Yet it must be noted that due to the small number of samples, the observed estimate is not significantly different from the other error estimates.

It is worth mentioning that a 0.3% uncertainty is expected from the temperature dependence of the line strengths of $^{16}O_3$. Due to the relatively high lower state energies of the transitions used for the measurement of the main isotopomer, the temperature dependency of the line strength is dominated by the population of these lower states. This gives rise to the following dependence of the line strength error ΔS on the uncertainty in temperature ΔT

$$\frac{\Delta S}{S} = \frac{E''}{k_B T}\frac{\Delta T}{T}\,. \tag{5}$$

The relative error of the absorption signal due to line strength uncertainties $\Delta S/S$ is thus proportional to the relative error of the temperature $\Delta T/T$, with the lower state energy E'' in units of the thermal energy $k_B T$ being the proportionality factor $E''/k_B T$. In spectral windows II and III, where the lower state energy is about $E'' = 1750\,\text{cm}^{-1}$ on average, an uncertainty in the temperature of 0.1 K leads to roughly 0.3% uncertainty in the derived concentration of $^{16}O_3$. Because the cell temperature was monitored by several Pt-100 thermometers with a precision of about 0.1 K, the value of 0.3% appears to be a reasonable estimate for the precision of the isotopomer enrichments.

3.2 *Instrument comparison*

In order to assess the instrument accuracy, a comparison with mass spectrometer measurements was carried out. A MS cannot directly differentiate between asymmetric and symmetric molecules of the same isotopic composition. Direct comparison with MS measurements is therefore prevented. Mass balance, however, implies that the isotopomer specific enrichments must add up to their isotopologic

Sample	TDLAS		MS	
	$\varepsilon(^{16}O_2^{18}O)$	$\varepsilon(^{16}O_2^{17}O)$	$\varepsilon(^{16}O_2^{18}O)$	$\varepsilon(^{16}O_2^{17}O)$
1	18.2(4)	14.1(3)	18.7(3)	14.7(4)
2	18.0(3)	14.0(3)	18.3(3)	14.0(4)
3	17.9(2)	14.1(2)	17.3(3)	14.2(4)
$\overline{\varepsilon(X)}$	18.0(1)	14.1(1)	18.0(7)	14.3(3)

TABLE 3 Diode laser (TDLAS) derived and mass spectrometrically (MS) obtained total enrichments for three sample and reference pairs. Uncertainties are derived assuming correlated errors in the two symmetry species (TDLAS) or from repeatability of standard measurements (MS). Averages and standard deviations (σ_{n-1}) are given in the last row

equivalents. Taking ^{18}O containing ozone as an example, if – as in our case – the reference ozone deviates slightly from the statistical composition in the heavy isotopomers by $\gamma_8 = [^{16}O^{16}O^{18}O]/(2[^{16}O^{18}O^{16}O]) - 1$, the following relationship between isotopologue and isotopomer specific enrichments can be derived:

$$(3+2\gamma_8)\,\varepsilon\left(^{16}O_2{}^{18}O\right) = 2(1+\gamma_8)\,\varepsilon\left(^{16}O^{16}O^{18}O\right) + \varepsilon\left(^{16}O^{18}O^{16}O\right) . \quad (6)$$

Note, that for the assumption of a statistical distribution of isotopes between the two heavy symmetry species in the reference ozone ($\gamma_8 = 0$), this relation reduces to the more common equation [11, e.g.]

$$3\varepsilon\left(^{16}O_2{}^{18}O\right) = 2\varepsilon\left(^{16}O^{16}O^{18}O\right) + \varepsilon\left(^{16}O^{18}O^{16}O\right) . \quad (7)$$

Due to systematic uncertainties in the line intensities of heavy ozone isotopomers [11, 30], γ_8 (and – equivalently – γ_7) in the reference gas cannot be independently determined with sufficient precision. Modeling of the low pressure formation process [16], however, gives values of $\gamma_8 = -0.05$ and $\gamma_7 = -0.04$, with worst case uncertainties of the same size. This amounts to a maximum bias of the isotopologue enrichments of 0.2% for both, $^{16}O_2^{18}O$ and $^{16}O_2^{17}O$ – still being less than the systematic 0.3% derived from temperature induced intensity uncertainties. Deriving isotopologue enrichments $\varepsilon(^{16}O_2{}^{18}O)$ and $\varepsilon(^{16}O_2{}^{17}O)$ from the individual isotopomers thus provides an indirect means to test the accuracy of the isotopomer abundance measurements within this limit. This is because errors in the different isotopomers are likely to add and not to cancel when the isotopomer enrichments are combined to yield the total isotopologue enrichment. The comparison of the above ozone samples with the mass spectrometrically obtained isotopologue enrichment values is given in Table 3.

A scale-expansion factor was applied to the MS data, which results in a correction of roughly 0.8% and 0.3% for $^{16}O_2{}^{17}O$ and $^{16}O_2{}^{18}O$, respectively. The scaling factor has been determined in a comparison with a high precision isotope ratio MS on oxygen gases having about the same isotopic compositions than the sample and reference gases. Though usually of much smaller size, non-ideal dynamic behaviour of mass spectrometers may frequently be observed. Despite being difficult to localise, these effects are commonly believed to be due to cross contamination and therefore are most pronounced when isotopic compositions of the sample and reference gases differ greatly [33]. When this correction is applied, good agreement between the two methods is obtained.

A t-test analysis on a significance level of 0.1 confirms that the agreement between the two methods is indeed quantitative and that the error estimate of 0.3% (1σ) is a reasonable number for the accuracy of the TDLAS. We conclude this discussion with the remark that despite the large span in the isotopic compositions between sample and reference ozone, no correction needs to be applied to the TDLAS results.

4 Conclusions and outlook

We have developed a new TDLAS for symmetry selective detection of ozone isotopomers. It was demonstrated that all ^{17}O and ^{18}O mono-substituted isotopomers can be simultaneously analysed with a precision of 6‰ (2σ). The instrument performance was validated by a comparison with MS measurements.

Presently, precision and accuracy of the spectrometer appears to be limited by two factors. Firstly, there is the strong temperature dependence of the line strengths of $^{16}O_3$. Improvements are expected from advancing the temperature control of the absorption cell. Even more feasible would be the addition of a second light path [21, 22, 34], the addition of one or more lasers [23] or a combination of both [20]. Either modification increases the choice of available lines and allows inclusion of lines of less temperature dependent intensities. Secondly, there is some uncertainty in the composition of the reference gas with regard to the symmetry species. If samples need to be well characterised, either the composition of the reference ozone with respect to a molecular oxygen standard or ozone line intensities must be known precisely. This issue is currently under investigation.

The precision obtained, however, is already sufficient for a symmetry resolved study of isotope effects in ozone formation. The possibility of simultaneously measuring ^{17}O and ^{18}O containing ozone opens up new pathways in the investigation of the unusual isotope effect and into the study of the transfer of the anomaly to other species. The first measurements on ^{17}O containing ozone presented here apparently confirm the assumption that the enrichment resides in the asymmetric molecule. More quantitative results will come from experiments where ozone is formed under well defined temperature conditions. Because asymmetric ozone is the source of heavy $O(^1D)$ in the atmosphere, $O(^1D)$ mediated isotope transfer into stratospheric CO_2 can now be studied at a much greater level of detail than before. In particular, isotope effects related to ozone can be separated from other effects, thus allowing addressing of the question [6], of whether the transfer steps introduce an additional anomaly or not?

ACKNOWLEDGEMENTS We are particularly grateful to R. Shaheen and T. Röckmann who made the mass spectrometer comparison possible by performing companion measurements on a high precision isotope ratio mass spectrometer.

REFERENCES

1 J. Morton, J. Barnes, B. Schueler, K. Mauersberger, J. Geophys. Res. **95**, 901 (1990)
2 S.M. Anderson, D. Hülsebusch, K. Mauersberger, J. Chem. Phys. **107**, 5385 (1997)
3 C. Janssen, J. Guenther, K. Mauersberger, D. Krankowsky, Phys. Chem. Chem. Phys. **3**, 4718 (2001)
4 K. Mauersberger, Geophys. Res. Lett. **8**, 935 (1981)

5 R.E. Weston, Chem. Rev. **99**, 2115 (1999)
6 C.A.M. Brenninkmeijer, C. Janssen, J. Kaiser, T. Röckmann, T.S. Rhee, S.S. Assonov, Chem. Rev. **103**, 5125 (2003)
7 K. Mauersberger, D. Krankowsky, C. Janssen, R. Schinke, In: B. Bederson, H. Walther (Eds.): Adv. Atom. Mol. Opt. Phys. Vol. 50 (Elsevier, 2005)
8 K. Mauersberger, P. Lämmerzahl, D. Krankowsky, Geophys. Res. Lett. **28**, 3155 (2001)
9 D. Krankowsky, F. Bartecki, G.G. Klees, K. Mauersberger, K. Schellenbach, J. Stehr, Geophys. Res. Lett. **22**, 1713 (1995)
10 T.B. Coplen, J.K. Böhlke, P. De Bièvre, T. Ding, N.E. Holden, J.A. Hopple, H.R. Krouse, A. Lamberty, H.S. Peiser, K. Révész, S.E. Rieder, K.J.R. Rosman, E. Roth, P.D.P. Taylor, R.D. Vocke, Jr., Y.K. Xiao, Pure Appl. Chem. **74**, 1987 (2002)
11 C. Janssen, J. Geophys. Res. **110**, D08308, doi 10.1029/2004JD005479 (2005)
12 T. Röckmann, J. Kaiser, J.N. Crowley, C.A.M. Brenninkmeijer, P.J. Crutzen, Geophys. Res. Lett. **28**, 503 (2001)
13 Y.L. Yung, A.Y.T. Lee, F.W. Irion, W.B. DeMore, J. Wen, J. Geophys. Res. **102**, 10 857 (1997)
14 A. Meier, J. Notholt, Geophys. Res. Lett. **23**, 551 (1996)
15 S.M. Anderson, J. Morton, K. Mauersberger, Chem. Phys. Lett. **156**, 175 (1989)
16 C. Janssen, J. Guenther, D. Krankowsky, K. Mauersberger, J. Chem. Phys. **111**, 7179 (1999)
17 R.W. Larsen, N.W. Larsen, F.M. Nicolaisen, G.O. Sørensen, J.A. Beukes, J. Mol. Spectrosc. **200**, 235 (2000)
18 D.G. Johnson, K.W. Jucks, W.A. Traub, K.V. Chance, J. Geophys. Res. **105**, 9025 (2000)
19 P. Bergamaschi, M. Bräunlich, T. Marik, C.A.M. Brenninkmeijer, J. Geophys. Res. **105**, 14 531 (2000)
20 K. Uehara, K. Yamamoto, T. Kikugawa, N. Yoshida, Spectrochim. Acta A **59**, 957 (2003)
21 J.B. McManus, M.S. Zahniser, D.D. Nelson, L.R. Williams, C.E. Kolb, Spectrochim. Acta A **58**, 2465 (2002)
22 D. Weidmann, G. Wysocki, C. Oppenheimer, F.K. Tittel, Appl. Phys. B **80**, 255 (2005)
23 L. Gianfrani, G. Gagliardi, M. van Burgel, E.R.T. Kerstel, Opt. Express **11**, 1566 (2003)
24 E. Kerstel, *Isotope Ratio Infrared Spectrometry* (Chap. 34), In: Handbook of Stable Isotope Analytical Techniques, P.A. de Groot (Ed.), (Elsevier, 2004) p. 759
25 F.K. Tittel, D. Richter, A. Fried, Top. Appl. Phys. **89**, 445 (2003)
26 B. Tuzson, C. Janssen, Isotopes Environ. Health Stud. (2005) accepted
27 M.S. Zahniser, B. McManus, pers. communication (2002)
28 L.S. Rothman, D. Jacquemart, A. Barbe, D.C. Benner, M. Birk, L.R. Brown, M.R. Carleer, C. Chackerian, K. Chance, L.H. Coudert, V. Dana, V.M. Devi, J.M. Flaud, R.R. Gamache, A. Goldman, J.M. Hartmann, K.W. Jucks, A.G. Maki, J.Y. Mandin, S.T. Massie, J. Orphal, A. Perrin, C.P. Rinsland, M.A.H. Smith, J. Tennyson, R.N. Tolchenov, R.A. Toth, J.V. Auwera, P. Varanasi, G. Wagner, J. Quant. Spectrosc. Radiat. Transfer, **96**, 139 (2005)
29 A.O. Nier, W.E. Potter, D.R. Hickman, K. Mauersberger, Radio Sci. **8**, 271 (1973)
30 J.M. Flaud, R. Bacis, Spectrochim. Acta A **54**, 3 (1998)
31 S.K. Bains-Sahota, M.H. Thiemens, J. Phys. Chem. **91**, 4370 (1987)
32 J.E. Heidenreich, M.H. Thiemens, J. Chem. Phys. **84**, 2129 (1986)
33 H.A.J. Meijer, R.E.M. Neubert, G.H. Visser, Int. J. Mass. Spectrom. **198**, 45 (2000)
34 K. Uehara, K. Yamamoto, T. Kikugawa, N. Yoshida, Sens. Actuators B **74**, 173 (2001)